

X-ray absorption and x-ray magnetic dichroism study on $\text{Ca}_3\text{CoRhO}_6$ and $\text{Ca}_3\text{FeRhO}_6$

T. Burnus,¹ Z. Hu,¹ Hua Wu,¹ J. C. Cezar,² S. Niitaka,^{3,4} H. Takagi,^{3,4,5} C. F. Chang,¹ N. B. Brookes,² H.-J. Lin,⁶ L. Y. Jang,⁶ A. Tanaka,⁷ K. S. Liang,⁶ C. T. Chen,⁶ and L. H. Tjeng¹

¹*II. Physikalisches Institut, Universität zu Köln, Zùlpicher Str. 77, 50937 Köln, Germany*

²*European Synchrotron Radiation Facility, BP 220, 38043, Grenoble, France*

³*RIKEN, Institute of Physical and Chemical Research, 2-1, Hirosawa, Wako, Saitama 351-0198, Japan*

⁴*CREST, Japan Science and Technology Agency (JST), Kawaguchi, Saitama 332-0012, Japan*

⁵*Department of Advanced Materials Science, University of Tokyo, 5-1-5, Kashiwanoha, Kashiwa, Chiba 277-8581, Japan*

⁶*National Synchrotron Radiation Research Center, 101 Hsin-Ann Road, Hsinchu 30077, Taiwan*

⁷*Department of Quantum Matter, ADSM, Hiroshima University, Higashi-Hiroshima 739-8530, Japan*

(Dated: October 22, 2018)

Using x-ray absorption spectroscopy at the Rh- $L_{2,3}$, Co- $L_{2,3}$, and Fe- $L_{2,3}$ edges, we find a valence state of $\text{Co}^{2+}/\text{Rh}^{4+}$ in $\text{Ca}_3\text{CoRhO}_6$ and of $\text{Fe}^{3+}/\text{Rh}^{3+}$ in $\text{Ca}_3\text{FeRhO}_6$. X-ray magnetic circular dichroism spectroscopy at the Co- $L_{2,3}$ edge of $\text{Ca}_3\text{CoRhO}_6$ reveals a giant orbital moment of about $1.7\mu_B$, which can be attributed to the occupation of the minority-spin d_0d_2 orbital state of the high-spin Co^{2+} ($3d^7$) ions in trigonal prismatic coordination. This active role of the spin-orbit coupling explains the strong magnetocrystalline anisotropy and Ising-like magnetism of $\text{Ca}_3\text{CoRhO}_6$.

PACS numbers: 78.70.Dm, 71.27.+a, 71.70.-d, 75.25.+z

I. INTRODUCTION

The quasi one-dimensional transition-metal oxides Ca_3ABO_6 ($A = \text{Fe, Co, Ni, } \dots$; $B = \text{Co, Rh, Ir, } \dots$) have attracted a lot of interest in recent years because of their unique electronic and magnetic properties.^{1,2,3,4,5,6,7,8,9,10,11,12,13} The structure of Ca_3ABO_6 contains one-dimensional (1D) chains consisting of alternating face-sharing AO_6 trigonal prisms and BO_6 octahedra. Each chain is surrounded by six parallel neighboring chains forming a triangular lattice in the basal plane. Peculiar magnetic and electronic behaviors are expected to be related to geometric frustration in such a triangle lattice with antiferromagnetic (AFM) interchain interaction and Ising-like ferromagnetic (FM) intrachain coupling. $\text{Ca}_3\text{Co}_2\text{O}_6$, which realizes such a situation, shows stair-step jumps in the magnetization at regular intervals of the applied magnetic field of $M_s/3$, suggesting ferrimagnetic spin alignment. It has a saturation magnetization of $M_s = 4.8\mu_B$ per formula unit at around 4 T.¹⁴ Studies on the temperature and magnetic-field dependence of the characteristic spin-relaxation time suggest quantum tunneling of the magnetization similar to single-molecular magnets.¹⁵ An applied magnetic field induces a large negative magnetoresistance, apparently not related to the three-dimensional magnetic ordering.¹¹ Band-structure calculations using the local-spin-density approximation plus Hubbard U (LSDA+U) predicted that the Co^{3+} ion at the trigonal site, being in the high-spin (HS) state ($S = 2$), has a giant orbital moment of $1.57\mu_B$ due to the occupation of minority-spin d_2 orbital, while the Co^{3+} ion at the octahedral site is in the low-spin (LS) state ($S = 0$).¹⁶ An x-ray absorption and magnetic circular dichroism study at the Co- $L_{2,3}$ edge has confirmed this prediction.¹⁷ Both studies explain well the Ising nature of the magnetism of $\text{Ca}_3\text{Co}_2\text{O}_6$.

$\text{Ca}_3\text{CoRhO}_6$ and $\text{Ca}_3\text{FeRhO}_6$ have the same crystal structure as $\text{Ca}_3\text{Co}_2\text{O}_6$, but different magnetic and electronic properties: Neutron diffraction and magnetization measurements also indicated intrachain-FM and interchain-AFM interactions in $\text{Ca}_3\text{CoRhO}_6$ like in $\text{Ca}_3\text{Co}_2\text{O}_6$.⁷ In contrast, susceptibility data on $\text{Ca}_3\text{FeRhO}_6$ reveal a single transition into a three-dimensional AFM.^{5,18} Although $\text{Ca}_3\text{CoRhO}_6$ has a similar magnetic structure as $\text{Ca}_3\text{Co}_2\text{O}_6$, it exhibits considerable differences in the characteristic temperatures in the magnetic susceptibility. The high-temperature limit of the magnetic susceptibility shows a Curie-Weiss behavior with a positive Weiss temperature of 150 K for $\text{Ca}_3\text{CoRhO}_6$,⁵ while 30 K was found for $\text{Ca}_3\text{Co}_2\text{O}_6$.^{2,3} The measured magnetic susceptibility undergoes two transitions at $T_{c_1} = 90$ K and $T_{c_2} = 25$ K for $\text{Ca}_3\text{CoRhO}_6$, and at $T_{c_1} = 24$ K and $T_{c_2} = 12$ K for $\text{Ca}_3\text{Co}_2\text{O}_6$,^{3,5,7,8,12,18} which were attributed to FM-intrachain and AFM-interchain coupling, respectively. In contrast, $\text{Ca}_3\text{FeRhO}_6$ has an AFM ordering below $T_N = 12$ K.^{5,18,19} Unlike $\text{Ca}_3\text{Co}_2\text{O}_6$, there is only one plateau at 4 T and no saturation even at 18 T in the magnetization of $\text{Ca}_3\text{CoRhO}_6$ at 70 K.⁷ A partially disordered state in $\text{Ca}_3\text{CoRhO}_6$ has been inferred by the previous work of Niitaka *et al.*⁸

In order to understand the contrasting magnetic properties of $\text{Ca}_3\text{CoRhO}_6$ and $\text{Ca}_3\text{FeRhO}_6$, and, particularly, the type and origin of the intrachain magnetic coupling of these quasi 1D systems, the valence, spin, and orbital states have to be clarified. However, these issues have been contradictorily discussed in previous theoretical and experimental studies. The general-gradient-approximated (GGA) density-functional band calculations²⁰ suggest a $\text{Co}^{3+}/\text{Rh}^{3+}$ state in $\text{Ca}_3\text{CoRhO}_6$, while LSDA+U calculations with inclusion of the spin-orbit coupling favor a $\text{Co}^{2+}/\text{Rh}^{4+}$

state and, again, a giant orbital moment due to the occupation of minority-spin d_0 and d_2 orbitals.²¹ Neutron diffraction experiments on $\text{Ca}_3\text{CoRhO}_6$ ^{8,22} suggest the $\text{Co}^{3+}/\text{Rh}^{3+}$ state. However, based on the magnetic susceptibility⁵ and x-ray photoemission spectroscopy²³ the $\text{Co}^{2+}/\text{Rh}^{4+}$ state was proposed. For $\text{Ca}_3\text{FeRhO}_6$, the $\text{Fe}^{2+}/\text{Rh}^{4+}$ state was suggested in a magnetic susceptibility study,⁵ whereas Mössbauer spectroscopy indicates a Fe^{3+} state,¹⁹ and thus Rh^{3+} .

In order to settle the above issues, in this work we first clarify the valence state of the Rh, Co, and Fe ions in $\text{Ca}_3\text{CoRhO}_6$ and $\text{Ca}_3\text{FeRhO}_6$ using x-ray absorption spectroscopy (XAS) at the $L_{2,3}$ edges of Rh, Co, and Fe. We reveal a valence state of $\text{Co}^{2+}/\text{Rh}^{4+}$ in $\text{Ca}_3\text{CoRhO}_6$ and of $\text{Fe}^{3+}/\text{Rh}^{3+}$ in $\text{Ca}_3\text{FeRhO}_6$. Then, we investigate the orbital occupation and magnetic properties using x-ray magnetic circular dichroism (XMCD) experiments at the Co- $L_{2,3}$ edge of $\text{Ca}_3\text{ChRhO}_6$. We find a minority-spin d_0d_2 occupation for the HS Co^{2+} ground state and, thus, a giant orbital moment of about $1.7\mu_B$. As will be seen below, our results account well for the previous experiments.

II. EXPERIMENTAL

Polycrystalline samples were synthesized by a solid-state reaction and characterized by x-ray diffraction to be single phase.⁵ The Rh- $L_{2,3}$ XAS spectra were measured at the NSRRC 15B beamline in Taiwan, which is equipped with a double-Si(111) crystal monochromator for photon energies above 2 keV. The photon-energy resolution at the Rh- $L_{2,3}$ edge ($h\nu \approx 3000\text{--}3150$ eV) was set to 0.6 eV. The Fe- $L_{2,3}$ XAS spectrum of $\text{Ca}_3\text{FeRhO}_6$ was measured at the NSRRC Dragon beamline with a photon-energy resolution of 0.25 eV. The main peak at 709 eV of the Fe- L_3 edge of single crystalline Fe_2O_3 was used for energy calibration. The Co- $L_{2,3}$ XAS and XMCD spectra of $\text{Ca}_3\text{CoRhO}_6$ were recorded at the ID8 beamline of ESRF in Grenoble with a photon-energy resolution of 0.2 eV. The sharp peak at 777.8 eV of the Co- L_3 edge of single crystalline CoO was used for energy calibration. The Co- $L_{2,3}$ XMCD spectra were recorded in a magnetic field of 5.5 T; the photons were close to fully circularly polarized. The sample pellets were cleaved *in situ* in order to obtain a clean surface. The pressure was below 5×10^{-10} mbar during the measurements. All data were recorded in total-electron-yield mode.

III. XAS AND VALENCE STATE

We first concentrate on the valence of the rhodium ions in both studied compounds. For $4d$ transition-metal oxides, the XAS spectrum at the $L_{2,3}$ edge reflects basically the unoccupied t_{2g} - and e_g -related peaks in the O_h symmetry. This is due to the larger band-like character and the stronger crystal-field interaction of the $4d$

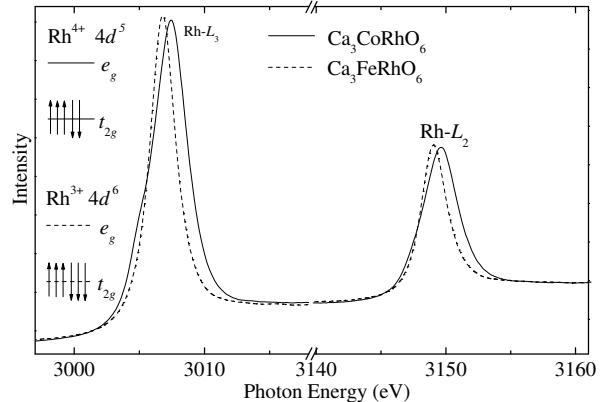


FIG. 1: The Rh- $L_{2,3}$ XAS spectra of $\text{Ca}_3\text{CoRhO}_6$ and $\text{Ca}_3\text{FeRhO}_6$ and a schematic energy level diagram for $\text{Rh}^{3+} 4d^6$ and $\text{Rh}^{4+} 4d^5$ configurations in octahedral symmetry.

states as well as due to the weaker intra-atomic interactions as compared with $3d$ transition-metal oxides, where intra-atomic multiplet interactions are dominant. The intra-atomic multiplet and spin-orbit interactions in $4d$ elements only modify the relative intensity of the t_{2g} - and e_g -related peaks. Fig. 1 shows the XAS spectra at the Rh- $L_{2,3}$ edges of $\text{Ca}_3\text{FeRhO}_6$ (dashed line) and $\text{Ca}_3\text{CoRhO}_6$ (solid line). The Rh- $L_{2,3}$ spectrum shows a simple, single-peaked structure at both Rh- L_2 and Rh- L_3 edges for $\text{Ca}_3\text{FeRhO}_6$, while an additional low-energy shoulder is observed for $\text{Ca}_3\text{CoRhO}_6$. Furthermore, the peak in the $\text{Ca}_3\text{CoRhO}_6$ spectrum is shifted by 0.8 eV to higher energies compared to that of the $\text{Ca}_3\text{FeRhO}_6$.

The single-peaked spectral structure for $\text{Ca}_3\text{FeRhO}_6$ indicates $\text{Rh}^{3+} (4d^6)$ with completely filled t_{2g} orbitals, i.e. only transitions from the $2p$ core levels to the e_g states are possible. The results are in agreement with Mössbauer spectroscopy.¹⁹ The shift to higher energies from $\text{Ca}_3\text{FeRhO}_6$ to $\text{Ca}_3\text{CoRhO}_6$ reflects the increase in the Rh valence from Rh^{3+} to Rh^{4+} as we can learn from previous studies on $4d$ transition-metal compounds.^{24,25,26,27} Furthermore, for $\text{Ca}_3\text{CoRhO}_6$ the spectrum shows a weak low-energy shoulder, which is weaker at the Rh- L_2 edge than at the Rh- L_3 edge. This shoulder can be attributed to transitions from the $2p$ core levels to the t_{2g} state, reflecting a $4d^5$ configuration with one hole at the t_{2g} state. Such spectral features were found earlier for Ru^{3+} in $\text{Ru}(\text{NH}_4)_3\text{Cl}_6$.^{24,28} Detailed calculations reveal that the multiplet and spin-orbit interactions suppress the t_{2g} -related peak at the L_2 edge for a $4d^5$ configuration.^{24,25,26,27} Thus, we find a $\text{Rh}^{4+} (4d^5)$ state for $\text{Ca}_3\text{CoRhO}_6$. Having determined a Rh^{3+} state in $\text{Ca}_3\text{FeRhO}_6$ and a Rh^{4+} state in $\text{Ca}_3\text{CoRhO}_6$, we turn to the Fe- $L_{2,3}$ and the Co- $L_{2,3}$ XAS spectra to further confirm the Fe^{3+} state and the Co^{2+} state, as expected for charge balance.

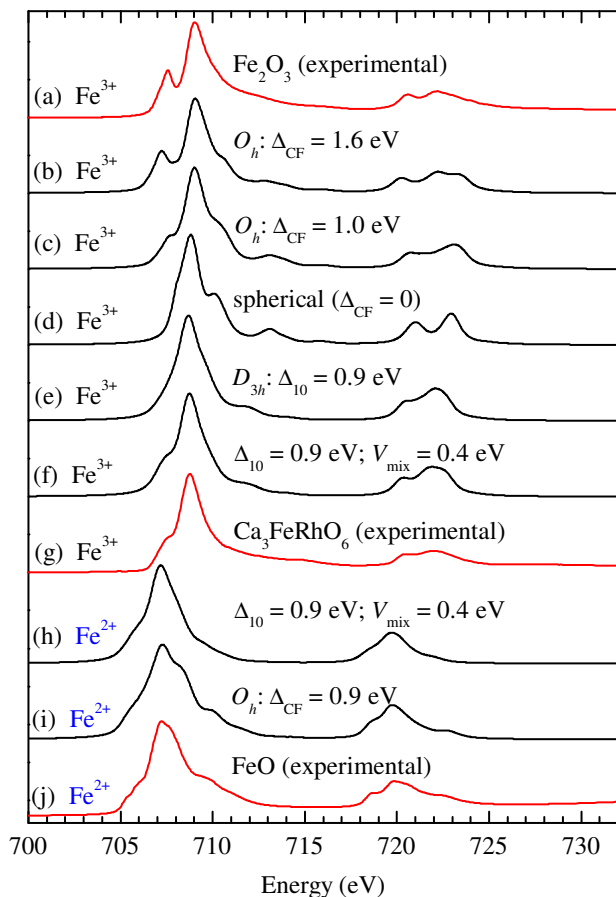


FIG. 2: (color online) Experimental XAS spectra at the Fe- $L_{2,3}$ edge of (a) Fe₂O₃ (Fe³⁺), (g) Ca₃FeRhO₆, and (j) FeO (Fe²⁺), taken from Park,²⁹ together with simulated spectra (b, c) in O_h , (d) spherical, and (e, f) D_{3h} symmetry for Fe³⁺ and simulated spectra in (h) D_{3h} and (i) O_h symmetry for Fe²⁺.

Figure 2 shows the experimental Fe- $L_{2,3}$ XAS spectra of (g) Ca₃FeRhO₆, along with those of (a) single crystalline Fe₂O₃ as a Fe³⁺ reference and of (j) FeO, taken from Ref. 29, as a Fe²⁺ reference. Additionally, calculated spectra for different symmetries using purely ionic crystal-field multiplet calculations^{24,30,31,32} are shown. It is well known that an increase of the valence state of the 3d transition-metal ion by one causes a shift of the XAS $L_{2,3}$ spectra by about one eV towards higher energies.^{33,34,35} The main peak of the Fe L_3 structure of the Ca₃FeRhO₆ lies 0.8 eV above the main peak of the divalent reference FeO and only slightly lower in energy than the one of Fe₂O₃ (Fe³⁺). This indicates trivalent iron ions in Ca₃FeRhO₆. The slightly lower energy shift of Ca₃FeRhO₆ relative to Fe₂O₃ can be attributed to the weak trigonal crystal field in the former as compared an octahedral field in the later, as we will show below.

The experimental spectra of the reference compounds, curve (a) for Fe₂O₃ and curve (j) for FeO, can be well understood using the multiplet calculations. For Fe₂O₃ we

find a good simulation taking a Fe³⁺ ion in an octahedral symmetry with a t_{2g} - e_g splitting of 1.6 eV, which is depicted in curve (b) in Fig. 2. For FeO, a good match with the experiment can be found for the Fe²⁺ in an octahedral environment with a splitting of 0.9 eV, see curve (i). The weaker crystal field in FeO, compared with Fe₂O₃, is consistent due to its larger Fe-O bond length.

In order to understand the experimental Fe $L_{2,3}$ spectrum of Ca₃FeRhO₆, we first return to the Fe₂O₃ spectrum. When we reduce the t_{2g} - e_g splitting from 1.6 eV (curve b) via 1.0 eV (curve c) to 0.0 eV (curve d), we observe that the the low-energy shoulder becomes washed out, while the high-energy shoulder becomes more pronounced.³⁰ Going further to a trigonal crystal field, the high-energy shoulder loses its intensity as shown in curve (e) for a splitting of 0.9 eV between $d_{\pm 1}$ (d_{yz}/d_{zx}) and $d_0/d_{\pm 2}$ ($d_{3z^2-r^2}/d_{xy}/d_{x^2-y^2}$). The experimental Fe- $L_{2,3}$ XAS spectrum of Ca₃FeRhO₆ in Fig. 2(g) can be well reproduced with this trigonal crystal field of 0.9 eV and in addition a mixing parameter $V_{\text{mix}} = 0.4$ eV, which mixes the $d_{\pm 2}$ with the $d_{\mp 1}$ orbitals; the result for this Fe with the 3d⁵ high-spin configuration is presented in curve (f).

We note that curve (f) has been generated with the Fe in the trivalent state. As a check, we have also tried to fit the experimental spectrum of Ca₃FeRhO₆ using a divalent Fe ansatz. However, the simulation does not match, as is illustrated in curve (h), in which we have used the same trigonal crystal field splitting of 0.9 eV and mixing parameter of 0.4 eV. To conclude, the Fe- $L_{2,3}$ and Rh- $L_{2,3}$ XAS spectra of Ca₃FeRhO₆ firmly establish the Fe³⁺/Rh³⁺ scenario.

For the Ca₃CoRhO₆ system, the Rh- $L_{2,3}$ XAS spectra suggest that the Rh ions are tetravalent, implying that the Co ions should be divalent. To confirm this Co²⁺/Rh⁴⁺ scenario we have to study explicitly the valence of the Co ion. Fig. 3 shows the Co- $L_{2,3}$ XAS spectra of Ca₃CoRhO₆ together with CoO as a Co²⁺ and Ca₃Co₂O₆ as a Co³⁺ reference.¹⁷ Again we see a shift to higher energies from CoO to Ca₃Co₂O₆ by about one eV. The Ca₃CoRhO₆ spectrum lies at the same energy position as the CoO spectrum confirming the Co²⁺/Rh⁴⁺ scenario²¹ and ruling out the Co³⁺/Rh³⁺ scenario.²⁰ The result is fully consistent with the above finding from the Rh- $L_{2,3}$ edge of Ca₃CoRhO₆ and in agreement with previous results from x-ray photoemission spectroscopy.²³

IV. XMCD AND ORBITAL OCCUPATION/MOMENT

After determining the valence states of Rh, Fe, and Co ions we turn our attention to the orbital occupation and magnetic properties of the Co²⁺ ion at the trigonal-prism site. This is motivated by the consideration that Co²⁺ ions may have a large orbital moment,³⁶ whose size depends on details of the crystal field, while the high-spin Fe³⁺ (3d⁵) and low-spin Rh³⁺ (4d⁶) ions in Ca₃FeRhO₆

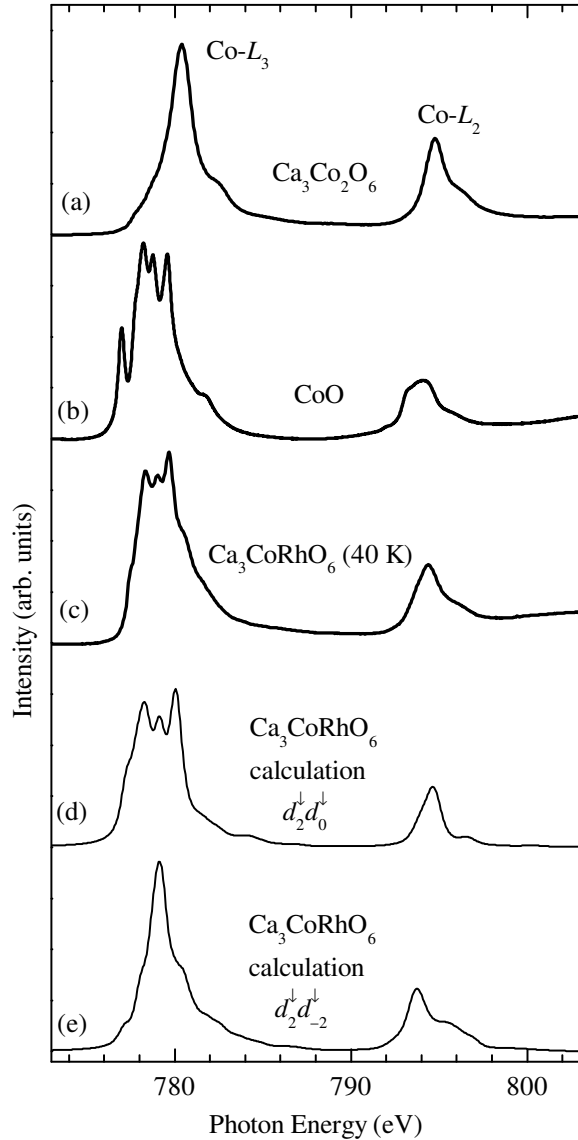


FIG. 3: The Co- $L_{2,3}$ spectra of (a) $\text{Ca}_3\text{Co}_2\text{O}_6$ (Co^{3+}), (b) CoO (Co^{2+}), and (c) $\text{Ca}_3\text{CoRhO}_6$. The simulated spectra of high-spin Co^{2+} ($3d^7$) in trigonal prismatic symmetry are shown in (d) for a d_0d_2 and in (e) for a d_2d_{-2} minority-spin orbital occupation.

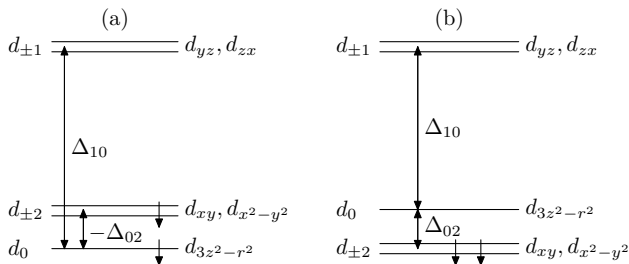


FIG. 4: Scheme of the two possible $3d$ occupations for a high-spin Co^{2+} ion in trigonal prismatic symmetry, ignoring the five up spins. (a) The d_0d_2 minority-spin occupation allows for a large orbital magnetic moment, whereas (b) for d_2d_{-2} the orbital moment vanishes.

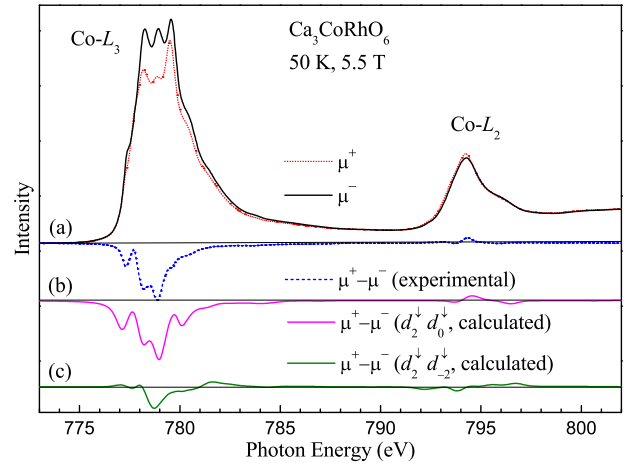


FIG. 5: (color online) (a) Measured soft x-ray absorption spectra with parallel (μ^+ , red dotted curve) and antiparallel (μ^- , black solid curve) alignment between photon spin and magnetic field, together with their difference (XMCD) spectrum ($\mu^+ - \mu^-$, blue dashed curve); simulated XMCD spectra for (b) d_0d_2 (olive curve) and (c) d_2d_{-2} (magenta curve) minority-spin occupation of the high-spin Co^{2+} .

have a closed subshell without orbital degrees of freedom and thus no orbital moment.

In trigonal-prism symmetry the $3d$ orbitals are split into $d_{\pm 1}$, d_0 , and $d_{\pm 2}$ states, see Fig. 4. In terms of one-electron levels, the $d_{\pm 1}$ orbitals lie highest in energy, while the lower lying d_0 , and $d_{\pm 2}$ usually are nearly degenerate. For a Co^{3+} d^6 system, it is *a priori* not obvious from band structure calculations to say which of these low lying orbitals gets occupied. Details, such as the inclusion of the spin-orbit interaction, can become crucial. Indeed, for $\text{Ca}_3\text{Co}_2\text{O}_6$, it was found from LDA+U calculations¹⁶ and confirmed by XMCD measurements¹⁷ that the spin-orbit interaction is crucial to stabilize the occupation of the d_2 orbital, thereby giving rise to giant orbital moments and Ising-type magnetism. For a Co^{2+} d^7 ion, however, the situation is quite different. As we will explain below, the double occupation of the d_0d_2 orbitals is energetically much more favored than that of the d_2d_{-2} : the energy difference could be of order 1 eV while the d_0 and $d_{\pm 2}$ by themselves could be degenerate on a one-electron level. The consequences are straightforward: the double occupation of d_0d_2 , see Fig. 4(a), should lead to a large orbital moment of $2\mu_B$ (neglecting covalent effects) and Ising type of magnetism with the magnetization direction fixed along the chains.^{7,21} In contrast, the d_2d_{-2} , see Fig. 4(b), would have given a quenched orbital moment.

In order to experimentally establish that the Co^{2+} ion has the d_0d_2 configuration, we have performed an XMCD study at the Co- $L_{2,3}$ edges of $\text{Ca}_3\text{CoRhO}_6$. Fig. 5 shows the Co- $L_{2,3}$ XMCD spectrum of $\text{Ca}_3\text{CoRhO}_6$ taken at 50 K under 5.5 T. The spectra were taken, respectively, with the photon spin parallel (μ^+ , red dotted curve) and

antiparallel (μ^- , black solid curve) to the magnetic field. One can clearly observe large differences between the two spectra with the different alignments. Their difference, $\mu^+ - \mu^-$, is the XMCD spectrum (blue dashed curve). An important feature of XMCD experiments is that there are sum rules, developed by Thole and Carra *et al.*,^{37,38} to determine the ratio between the orbital ($m_{\text{orb}} = L_z$) and spin ($m_{\text{spin}} = 2S_z$) contributions to the magnetic moment, namely

$$\frac{m_{\text{orb}}}{m_{\text{spin}}} = \frac{2}{3} \frac{\Delta L_3 + \Delta L_2}{\Delta L_3 - 2\Delta L_2}, \quad (1)$$

here, ΔL_3 and ΔL_2 are the energy integrals of the L_3 and L_2 XMCD intensity. The advantage of these sum rules is that one needs not to do any simulations of the spectra to obtain the desired quantum numbers. In our particular case, we can immediately recognize the presence of a large orbital moment in Fig. 5(a), since there is a large net (negative) integrated XMCD spectral weight. Using Eq. (1) we find $m_{\text{orb}}/m_{\text{spin}} = 0.63$. Since the Co^{2+} ion is quite ionic, m_{spin} is very close to the expected ionic value of $3\mu_B$. For example, our LDA+U calculations yield $2.72\mu_B$ for the Co^{2+} ion ($2.64\mu_B$ for LDA) and Whangbo *et al.* obtained $2.71\mu_B$ from GGA calculations.²⁰ Using a value of $2.7\mu_B$ for the spin moment, we estimate $m_{\text{orb}} = 1.7\mu_B$, in nice agreement with our LDA+U result of $1.69\mu_B$, for the d_0d_2 minority-spin orbital occupation.²¹

To critically check our experimental and previous LDA+U results²¹ regarding the d_0d_2 orbital occupation and the giant orbital moment, we explicitly simulate the experimental XMCD spectra using a charge-transfer configuration-interaction cluster calculation,^{24,31,32} which includes not only the full atomic multiplet theory and the local effects of the solid, but also the oxygen $2p$ -cobalt $3d$ hybridization. The results of the calculated Co- $L_{2,3}$ XAS and XMCD spectra are presented in Figs. 3(d) and 5(b), respectively. We can clearly observe that the simulations reproduce the experimental spectra very well. The parameters³⁹ used are those which indeed give the d_0d_2 orbital occupation for the ground state. The magnetic quantum numbers found are $m_{\text{orb}} = 1.65\mu_B$ and $m_{\text{spin}} = 2.46\mu_B$, yielding $m_{\text{orb}}/m_{\text{spin}} = 0.67$ and a total Co magnetic moment of $4.11\mu_B$. With the Rh in the $S = 1/2$ tetravalent state, the total magnetic moment per formula unit should be around $5\mu_B$. This is not inconsistent with the results of the high-field magnetization study by Niitaka *et al.*⁷: they found a total moment of $4.05\mu_B$, but there the saturation of the magnetization has not yet been reached even under 18.7 Tesla. This can now be understood since the magnetocrystalline anisotropy, associated with the active spin-orbit coupling, is extremely strong and makes it difficult to fully magnetize a powder sample as was used in their study.

We also have simulated the spectra for the d_2d_{-2} scenario. These are depicted in Figs. 3(e) for the XAS

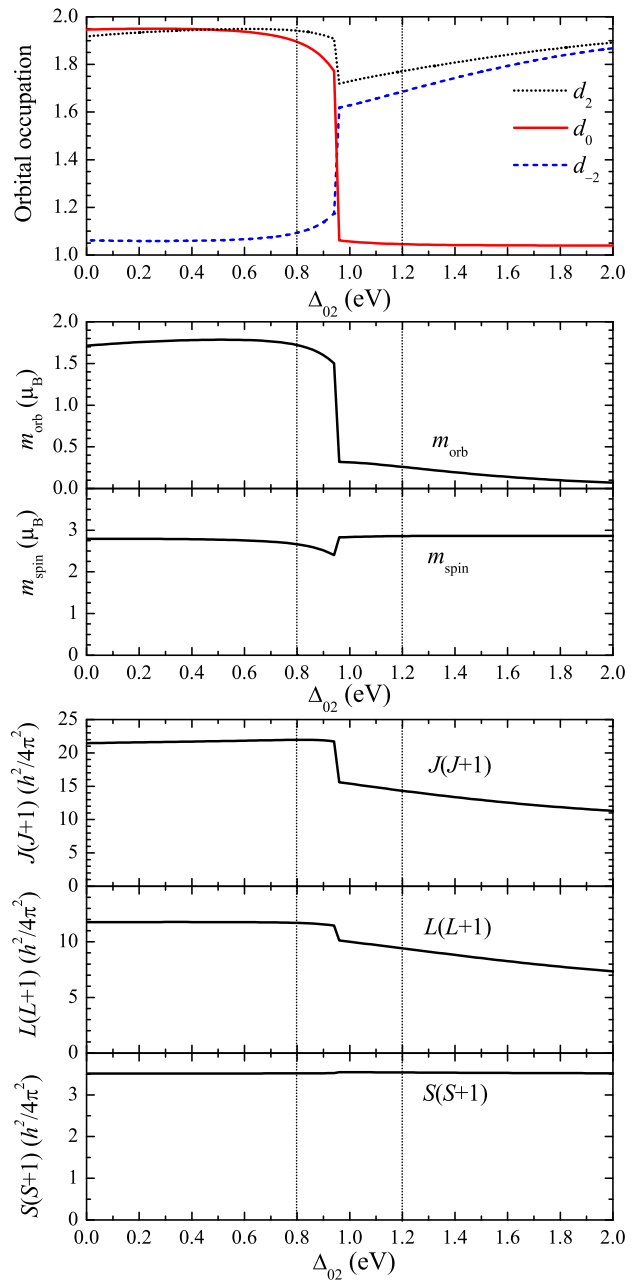


FIG. 6: (color online) Top panel: Occupation number of the d_0 , d_2 , and d_{-2} orbitals as function of the d_0 - $d_{\pm 2}$ splitting Δ_{02} [Fig. 4(b)]. Middle panel: Orbital and spin moments (m_{orb} and m_{spin}) as function of Δ_{02} . Bottom panel: $J(J+1)$, $L(L+1)$, and $S(S+1)$ as function of Δ_{02} .

and 5(c) for the XMCD. It is obvious that the experimental spectra are not reproduced. The simulated line shapes are very different from the experimental ones and the integral of the simulated XMCD spectrum yields a vanishing orbital moment. We therefore can safely conclude that the ground state of this material is not d_2d_{-2} . For completeness we mention that the magnetic quantum numbers found for this d_2d_{-2} ansatz are $m_{\text{orb}} = 0.03\mu_B$ and $m_{\text{spin}} = 2.86\mu_B$, yielding $m_{\text{orb}}/m_{\text{spin}} = 0.01$ and a

total Co magnetic moment of $2.89\mu_B$.

V. STABILITY OF THE d_2d_0 STATE

Having established that the ground state of $\text{Ca}_3\text{CoRhO}_6$ has the $\text{Co}^{2+} d^7$ ion in the doubly occupied d_0d_2 orbital configuration and not in the d_2d_{-2} , it is interesting to study its stability in more detail. As already mentioned above, for a $\text{Co}^{3+} d^6$ ion, the d_0 and $d_{\pm 2}$ states can be energetically very close to each other. For a $\text{Co}^{2+} d^7$ ion, however, the d_0d_2 and d_2d_{-2} states are very much different in energy. This is illustrated in the top panel of Fig. 6, in which we have calculated the occupation numbers of the d_0 , d_2 , and d_{-2} orbitals as a function of Δ_{02} , the one-electron level splitting between the d_0 and $d_{\pm 2}$ orbitals. The d_0d_2 ground state which gives the best simulation to the experimental XAS and XMCD spectra was obtained with $\Delta_{02} \approx 0.4$ eV. We can observe that the d_0d_2 situation is quite stable for a wide range of Δ_{02} values, certainly up to 0.8 eV. With a transition region between $\Delta_{02} = 0.8$ –1.2 eV, we find a stable d_2d_{-2} situation only for Δ_{02} values larger than 1.2 eV. (For the d_2d_{-2} simulations above we have used $\Delta_{02} = 1.4$ eV.) This is a very large number indeed, and it can be traced back to the multiplet character of the on-site Coulomb interactions: an occupation of d_2d_{-2} means a much stronger overlap of the electron clouds as compared to the case for a d_0d_2 . This results in a higher repulsion energy, which is not a small quantity in view of the atomic-like values of the F^2 and F^4 Slater integrals determining the multiplet splitting.^{31,40}

In the middle panel of Fig. 6 we also show the expectation values for m_{orb} and m_{spin} when varying Δ_{02} . Again we clearly observe that the large orbital-moment situation is quite stable. To quench the orbital moment

one would need much higher Δ_{02} values. Important is that the spin state does not change here. Bottom panel of Fig. 6 demonstrates that the high-spin state of the Co^{2+} ion is not affected by Δ_{02} : the expectation value $\langle S^2 \rangle$ remains constant throughout at a value consistent with an essentially $S = 3/2$ state. Obviously, the L^2 and J^2 quantum numbers are strongly affected by Δ_{02} .

VI. CONCLUSION

To summarize, the Rh- $L_{2,3}$, Co- $L_{2,3}$ and Fe- $L_{2,3}$ XAS measurements indicate $\text{Co}^{2+}/\text{Rh}^{4+}$ in $\text{Ca}_3\text{CoRhO}_6$ and $\text{Fe}^{3+}/\text{Rh}^{3+}$ in $\text{Ca}_3\text{FeRhO}_6$. The magnetic properties of $\text{Ca}_3\text{FeRhO}_6$ are relatively simple as both the HS Fe^{3+} and LS Rh^{3+} ions have a closed subshell and thus no orbital degrees of freedom and no orbital moment. The weak intrachain AFM coupling between the HS Fe ions can be understood in terms of the normal superexchange via the intermediate non-magnetic O–Rh–O complex. For $\text{Ca}_3\text{CoRhO}_6$, the combined experimental and theoretical study of the Co- $L_{2,3}$ XAS and XMCD spectra reveals a giant orbital moment of about $1.7\mu_B$. This large orbital moment is connected with the minority-spin d_0d_2 occupation for HS Co^{2+} ($3d^7$) ions in the peculiar trigonal prismatic coordination. The high FM ordering temperature in $\text{Ca}_3\text{CoRhO}_6$, compared with that of $\text{Ca}_3\text{Co}_2\text{O}_6$, can be attributed to the distinct octahedral sites (which mediate the Co–Co magnetic coupling): the magnetic Rh^{4+} ion ($S = 1/2$) in the former and the nonmagnetic Co^{3+} ion ($S = 0$) in the latter.

We would like to thank Lucie Hamdan for her skillful technical and organizational assistance in preparing the experiment. The research in Köln is supported by the Deutsche Forschungsgemeinschaft through SFB 608.

-
- ¹ H. Fjellvåg, E. Gulbrandsen, S. Aasland, A. Olsen, and B. C. Hauback, *J. Solid State Chem.* **124**, 190 (1996).
 - ² S. Aasland, H. Fjellvåg, and B. Hauback, *Solid State Commun.* **101**, 187 (1997).
 - ³ H. Kageyama, K. Yoshimura, K. Kosuge, H. Mitamura, and T. Goto, *J. Phys. Soc. Jpn.* **66**, 1607 (1997).
 - ⁴ H. Kageyama, K. Yoshimura, K. Kosuge, M. Azuma, M. Takano, H. Mitamura, and T. Goto, *J. Phys. Soc. Jpn.* **66**, 3996 (1997).
 - ⁵ S. Niitaka, H. Kageyama, M. Kato, K. Yoshimura, and K. Kosuge, *J. Solid State Chem.* **146**, 137 (1999).
 - ⁶ A. Maignan, C. Michel, A. C. Masset, C. Martin, and B. Raveau, *Euro. Phys. J. B* **15**, 657 (2000).
 - ⁷ S. Niitaka, H. Kageyama, K. Yoshimura, K. Kosuge, S. Kawano, N. Aso, A. Mitsuda, H. Mitamura, and T. Goto, *J. Phys. Soc. Jpn.* **70**, 1222 (2001).
 - ⁸ S. Niitaka, K. Yoshimura, K. Kosuge, M. Nishi, and K. Kakurai, *Phys. Rev. Lett.* **87**, 177202 (2001).
 - ⁹ B. Martínez, V. Laukhin, M. Hernando, J. Fontcuberta, M. Parras, and J. M. González-Calbet, *Phys. Rev. B* **64**, 012417 (2001).
 - ¹⁰ E. V. Sampathkumaran and A. Niazi, *Phys. Rev. B* **65**, 180401 (2002).
 - ¹¹ B. Raquet, M. N. Baibich, J. M. Broto, H. Rakoto, S. Lambert, and A. Maignan, *Phys. Rev. B* **65**, 104442 (2002).
 - ¹² V. Hardy, M. R. Lees, A. Maignan, S. Hébert, D. Flahaut, C. Martin, and D. Mc K. Paul, *J. Phys.: Condens. Matter* **15**, 5737 (2003).
 - ¹³ X. Yao, S. Dong, K. Xia, P. Li, and J.-M. Liu, *Phys. Rev. B* **76**, 024435 (2007).
 - ¹⁴ A. Maignan, V. Hardy, S. Hébert, M. Drillon, M. R. Lees, O. Petrenko, D. Mc K. Paul, and D. Khomskii, *J. Mater. Chem.* **14**, 1231 (2004).
 - ¹⁵ V. Hardy, D. Flahaut, M. R. Lees, and O. A. Petrenko, *Phys. Rev. B* **70**, 214439 (2004).
 - ¹⁶ H. Wu, M. W. Haverkort, Z. Hu, D. I. Khomskii, and L. H. Tjeng, *Phys. Rev. Lett.* **95**, 186401 (2005).
 - ¹⁷ T. Burnus, Z. Hu, M. W. Haverkort, J. C. Cezar, D. Flahaut, V. Hardy, A. Maignan, N. B. Brookes, A. Tanaka, H. H. Hsieh, et al., *Phys. Rev. B* **74**, 245111 (2006).

- ¹⁸ M. J. Davis, M. D. Smith, and H.-C. zur Loye, *J. Solid State Chem.* **173**, 122 (2003).
- ¹⁹ S. Niitaka, K. Yoshimura, K. Kosuge, K. Mibu, H. Mitamura, and T. Goto, *J. Magn. Magn. Mater.* **260**, 48 (2003).
- ²⁰ M.-H. Whangbo, D. Dai, H.-J. Koo, and S. Jovic, *Solid State Commun.* **125**, 413 (2003).
- ²¹ H. Wu, Z. Hu, D. I. Khomskii, and L. H. Tjeng, *Phys. Rev. B* **75**, 245118 (2007).
- ²² M. Loewenhaupt, W. Schäfer, A. Niazi, and E. V. Sampathkumaran, *Europhys. Lett.* **63**, 374 (2003).
- ²³ K. Takubo, T. Mizokawa, S. Hirata, J.-Y. Son, A. Fujimori, D. Topwal, D. D. Sarma, S. Rayaprol, and E. V. Sampathkumaran, *Phys. Rev. B* **71**, 073406 (2005).
- ²⁴ F. M. F. de Groot, Z. W. Hu, M. F. Lopez, G. Kaindl, F. Guillot, and M. Tronc, *J. Chem. Phys.* **101**, 6570 (1994).
- ²⁵ Z. Hu, H. von Lips, M. S. Golden, J. Fink, G. Kaindl, F. M. F. de Groot, S. Ebbinghaus, and A. Reller, *Phys. Rev. B* **61**, 5262 (2000).
- ²⁶ Z. Hu, M. S. Golden, S. G. Ebbinghaus, M. Knupfer, J. Fink, F. M. F. de Groot, and G. Kaindl, *Chem. Phys.* **282**, 451 (2002).
- ²⁷ R. K. Sahu, Z. Hu, M. L. Rao, S. S. Manoharan, T. Schmidt, B. Richter, M. Knupfer, M. Golden, J. Fink, and C. M. Schneider, *Phys. Rev. B* **66**, 144415 (2002).
- ²⁸ T. K. Sham, *J. Am. Chem. Soc.* **105**, 2269 (1983).
- ²⁹ J.-H. Park, Ph.D. thesis, University of Michigan (1994).
- ³⁰ F. M. F. de Groot, J. C. Fuggle, B. T. Thole, and G. A. Sawatzky, *Phys. Rev. B* **42**, 5459 (1990).
- ³¹ A. Tanaka and T. Jo, *J. Phys. Soc. Jpn.* **63**, 2788 (2004).
- ³² See the “Theo Thole Memorial Issue”, *J. Electron Spectrosc. Rel. Phenom.* **86**, 1 (1997).
- ³³ C. T. Chen and F. Sette, *Physica Scripta* **T31**, 119 (1990).
- ³⁴ C. Mitra, Z. Hu, P. Raychaudhuri, S. Wirth, S. I. Csiszar, H. H. Hsieh, H.-J. Lin, C. T. Chen, and L. H. Tjeng, *Phys. Rev. B* **67**, 092404 (2003).
- ³⁵ T. Burnus, Z. Hu, H. H. Hsieh, V. L. J. Joly, P. A. Joy, M. W. Haverkort, H. Wu, A. Tanaka, H.-J. Lin, C. T. Chen, et al., *Phys. Rev. B* **77**, 08xxxx (2008), (accepted). arXiv:0709.3243.
- ³⁶ G. Ghiringhelli, L. H. Tjeng, A. Tanaka, O. Tjernberg, T. Mizokawa, J. L. de Boer, and N. B. Brookes, *Phys. Rev. B* **66**, 075101 (2002).
- ³⁷ B. T. Thole, P. Carra, F. Sette, and G. van der Laan, *Phys. Rev. Lett.* **68**, 1943 (1992).
- ³⁸ P. Carra, B. T. Thole, M. Altarelli, and X. Wang, *Phys. Rev. Lett.* **70**, 694 (1993).
- ³⁹ Parameters (in eV). $U_{3d,3d} = 5$, $U_{2p,3d} = 6.5$, $\Delta = 4$, $\Delta_{10}^{\text{ionic}} = 0.65$, $V_{\text{mix}}^{\text{ionic}} = -0.2$, $V_{pd\sigma} = -1.024$, $H_{\text{ex}} = 0.045$. The Slater integrals were reduced to 80% of their Hartree-Fock value. $\Delta_{02}^{\text{ionic}} = 0.4$ (d_0d_2 scenario), $\Delta_{02}^{\text{ionic}} = 1.4$ (d_2d_{-2}).
- ⁴⁰ E. Antonides, E. C. Janse, and G. A. Sawatzky, *Phys. Rev. B* **15**, 1669 (1977).